[AMERICAN JOURNAL OF SCIENCE, SCHAIRER VOL. 267-A, 1969, P. 364-390]

DIOPSIDE + SPINEL EQUILIBRIA, ANORTHITE AND FORSTERITE REACTION RELATIONSHIPS IN SILICA-POOR LIQUIDS IN THE SYSTEM CaO–MgO–Al_2O_3–SiO_2 AT ATMOSPHERIC PRESSURE AND THEIR BEARING ON THE GENESIS OF MELILITITES AND NEPHELINITES

M. J. O'HARA and G. M. BIGGAR

Grant Institute of Geology

University of Edinburgh, Edinburgh, Scotland

ABSTRACT. Subsolidus charges consisting of anorthite + forsterite + melilite have been converted to diopside + spinel bearing assemblages in one month at 1200 to 1230°C. Three univariant (isobaric invariant) equilibria have been located: anorthite + forsterite + diopside + spinel + liquid at 1233.5 ± 1.5°C, forsterite + melilite + diopside + spinel + liquid between 1231 ± 1.0°C and 1233.5 ± 1.5°C, and anorthite + melilite + diopside + spinel + liquid at 1230 ± 0.5°C. An invariant equilibrium anorthite + forsterite + melilite + diopside + spinel + liquid may occur at a pressure below atmospheric and a temperature below 1230°C. This demonstration of the stability of the diopside + spinel assemblage at atmospheric pressure requires revisions of a number of published diagrams. Anorthite and forsterite are in reaction relationship with a silica-poor liquid in the first of the univariant equilibria referred to above, forsterite in the second, while the third is an eutectic. The reaction relationship between calcic plagioclase and liquid may persist into more complex systems analogous to the natural basic igneous rocks which are strongly undersaturated in silica, thereby permitting the derivation of melilite-nephelinites by low-pressure fractional crystallization of alkali-olivine basalts.

INTRODUCTION

At the outset of this study the five crystalline phases anorthite (an), forsterite (fo), melilite (mel), diopside (di), and spinel (sp) were known to be stable in the system CaO–MgO–Al_2O_3–SiO_2 (C-M-A-S) at solidus temperatures at atmospheric pressure and to have extensive primary phase volumes at the liquidus (Osborn and others, 1954).

All possible two-phase crystalline assemblages among the five phases were known to be stable at atmospheric pressures in the presence of large proportions of liquid (Osborn and others, 1954) except that of di + sp.

The stability at the solidus and liquidus of the three-phase crystalline assemblages an + di + fo, an + di + mel, an + fo + sp, an + sp + mel, and di + fo + mel had also been established (Osborn and others, 1954). None of the assemblages an + fo + mel, di + sp + an, di + sp + mel, or di + sp + fo had been observed in the presence of abundant liquid (l) under conditions that precluded the possibility of metastable crystallization, although the assemblage an + fo + mel had been produced repeatedly in the devitrification of glasses of suitable composition and displayed fritting at temperatures above 1180°C suggestive of the coexistence of an + fo + mel + liquid (Chinner and Schairer, 1962; de Neufville and Schairer, 1962).

If an + fo + mel + l is a stable assemblage di + sp + l cannot be, unless the invariant equilibrium of the quaternary system, involving an + fo + mel + di + sp + l ($^4E^0_{an,\ fo,\ mel,\ di,\ sp,\ l}$) occurs exactly at

atmospheric pressure (O'Hara and Schairer, 1963). (The shorthand notation used here has the general form ${}^{C}E^{F}_{P\,(named)}$: where C = number of components, F = degrees of freedom, P = number of phases, and P + F = C + 2). The tie-lines joining spinel (MA) and any likely diopside composition (CMS_2 plus moderate amounts of CAS and MAS) penetrate all possible tie-planes linking anorthite (CAS_2), forsterite (M_2S), and any melilite solid solution between akermanite (C_2MS_2) and gehlenite (C_2AS) as illustrated by figure 1 and equations 1, 2.

$$3CAS_2 + 4M_2S + 2C_2MS_2 = 7CMS_2 + 3MA \quad (1)$$

$$3CAS_2 + 6M_2S + 2C_2AS = 7CMS_2 + 5MA \quad (2)$$

It follows that either,

1. The subsolidus tetrahedra an + fo + mel + di and an + fo + mel + sp together with their univariant (isobaric invariant) melting equilibria ${}^{4}E^{1}_{an,\,fo,\,mel,\,di,\,1}$ and ${}^{4}E^{1}_{an,\,fo,\,mel,\,sp,\,1}$ and the divariant ${}^{4}E^{2}_{an,\,fo,\,mel,\,1}$ will be observed, yielding the form of the flow sheet preferred by Chinner and Schairer (1962, fig. 4, region near points C and D),

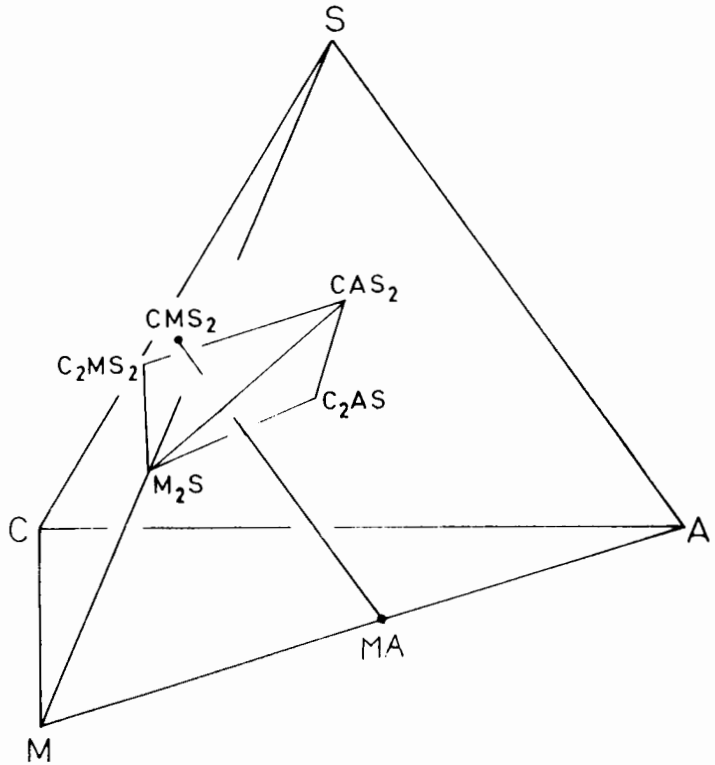

Fig. 1. System CMAS showing the relationship between the diopside (CMS_2)–spinel (MA) join and the anorthite (CAS_2)–forsterite (M_2S)–melilite (C_2MS_2–C_2AS) planes.

or 2. The subsolidus tetrahedra an + fo + di + sp, fo + mel + di + sp, and an + mel + di + sp, together with their associated uni-,di- and trivariant melting equilibria, $^4E^1_{an,\ fo,\ di,\ sp,\ l}$, $^4E^1_{fo,\ mel,\ di,\ sp,\ l}$, $^4E^1_{an,\ mel,\ di,\ sp,\ l}$, $^4E^2_{an,\ di,\ sp,\ l}$, $^4E^2_{fo,\ di,\ sp,\ l}$, $^4E^2_{mel,\ di,\ sp,\ l}$, and $^4E^3_{di,\ sp,\ l}$, will be observed, yielding the alternative form of the flow sheet discussed by O'Hara and Schairer (1963).

Chinner and Schairer (1962) reported the appearance of diopside in the presence of liquid at temperatures close to 1240°C in intermediate mixtures on the grossular (C_3AS_3)–pyrope (M_3AS_3) join, in charges which at higher temperatures contained spinel + liquid and at lower temperatures crystallized as an + fo + mel. It is impossible to contruct any plausible form of the phase diagram that will permit the appearance of spinel, its disappearance, and replacement by diopside to be followed by the disappearance of diopside and freezing to anorthite + forsterite + melilite as an equilibrium sequence of events on cooling. This led O'Hara and Schairer (1963) and Schairer and Kushiro (1965) to reinvestigate critical compositions on the joins C_3AS_3–M_3AS_3, CMS_2–CAS, and CMS_2–MA, where complex mineral assemblages persistently resulted from runs at about 1230 to 1240°C on initially glassy and on devitrified an + fo + mel bearing assemblages; an, fo, mel, di, and sp, all being present together with glass in many of the runs. The amount of diopside was invariably small, and this together with the very rapid growth and long persistence of metastable diopside solid solutions reported by O'Hara and Schairer (1963) cast doubts upon the stability of the diopside in these run products. O'Hara and Schairer (1963) were unable to resolve the problem, but Schairer and Kushiro (1965) reasoned from further data that an + fo + mel was probably stable and di + sp probably unstable, although they also were unable to prove the point beyond reasonable doubt.

If the an + fo + mel assemblage is stable, then the melilite composition in all the an + fo + mel bearing equilibria is close to akermanite 75 percent gehlenite 25 percent ($ak_{75}geh_{25}$) as demonstrated by de Neufville and Schairer (1962).

The composition plane C_3A–M–S within the system CMAS intersects the an–fo–mel tie-planes in such a way (fig. 1) that if an + fo + $ak_{75}geh_{25}$ is the stable assemblage coexisting with either diopside or spinel, the tie-plane will intersect the section C_3A–M–S as a straight line linking the forsterite composition (M_2S) to the piercing point of the join an + $ak_{75}geh_{25}$ (X in fig. 2). The tetrahedron an + fo + mel + di is intersected as a triangular area subtended to the silica-rich side by this line and the piercing point of the an–di join (Y in fig. 2). The tetrahedron an + fo + mel + sp is intersected as a triangular area subtended to the silica-poor side by this line and the piercing point of the sp + $ak_{75}geh_{25}$ join (Z in fig. 2).

The tie-planes an + di + mel, an + di+ fo, fo + mel + sp, and an + mel + sp are intersected as the straight lines bounding the large quadrilateral area so generated (figs. 2, 3). These are known to be

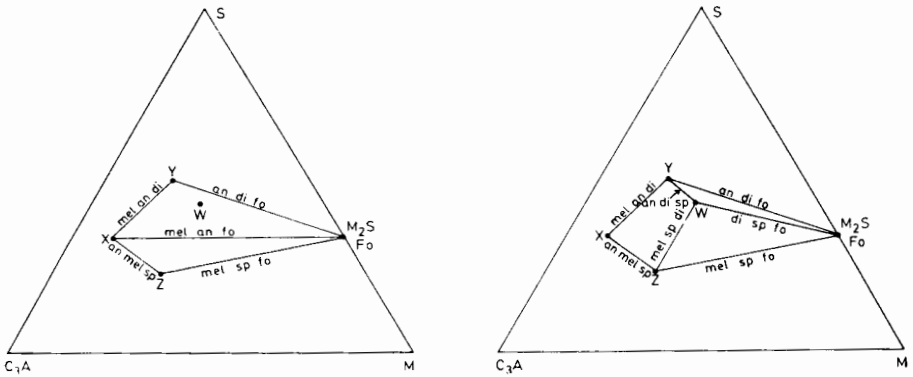

Figs. 2 and 3. The plane C_3A–M–S (schematic) showing the piercing points of the diopside-spinel join, W, the anorthite-melilite ($ak_{75}geh_{25}$) join, X, the anorthite–diopside join, Y, and the spinel-melilite ($ak_{75}geh_{25}$) join, Z, with the tie planes and subsolidus volumes encountered if anorthite + forsterite + melilite ($ak_{75}geh_{25}$) is the stable assemblage (fig. 2) or if diopside + spinel is the stable assemblage (fig. 3). Further explanation in the text.

stable assemblages even if an + fo + mel is not and is replaced by di + sp as shown in figure 3.

The di–sp join pierces the section C_3A–M–S within the large quadrilateral area and to the silica-rich side of the intersection with the plane an–fo–$ak_{75}geh_{25}$ (figs. 2, 3). If di + sp is stable the tie-planes an + di + sp, fo + di + sp, $ak_{75}geh_{25}$ + di + sp must also be stable and intersect the section C_3A–M–S as the three straight lines radiating from the di + sp piercing point (W) to the an + di piercing point (Y), the fo composition, and the sp + $ak_{75}geh_{25}$ piercing point (Z) respectively (fig. 3). The large quadrilateral area is thus divided up into two triangular areas and a small quadrilateral area meeting at the di + sp piercing point. The triangular area to the silica-rich side of the plane di + sp + fo is the intersection with the tetrahedron an + fo + di + sp; that to the silica-poor side is the intersection with the tetrahedron $ak_{75}geh_{25}$ + fo + di + sp, while the small quadrilateral W–Z–X–Y is the intersection of the tetrahedron an + $ak_{75}geh_{25}$ + di + sp with the section C_3A–M–S (fig. 3).

Subject to minor changes resulting from the presence of calcium in the forsterite in these equilibria and of solid solution of CAS, CS, and MAS molecules in the equilibrium diopside, either figure 2 or figure 3 may represent the equilibrium solidus assemblages developed in compositions lying in this region of the section C_3A–M–S.

NEW EXPERIMENTAL RESULTS

Figure 4 is a wt percent plot of the central section of the plane C_3A–M–S showing the piercing points and planes discussed in figures 2 and 3, together with extra information about the stable subsolidus assemblages developed at 1204 to 1230°C. It shows the positions of the piercing points in the section C_3A–M–S of the joins CMS_2–CAS, CMS_2–A,

CMS_2–MAS, and CMS_2–M_3AS_3 (diopside–Ca Tschermak's molecule, diopside–alumina, diopside–$MgAl_2SiO_6$, and diopside–pyrope respectively) which have been investigated by Schairer and co-workers at the Geophysical Laboratory since 1960.

Figure 4 shows and table 3 lists the compositions studied within the area of interest of the section C_3A–M–S. These compositions have been made up and studied as part of a much larger program covering the section C_3A–M–S in a series of pseudobinary joins radiating from the M apex, results from which are not yet complete.

Ten grams of each composition were made up by a gel technique from purest available starting materials. The gels were dehydrated and crystallized at moderate temperatures culminating in a treatment of more than 16 hours at 1050 to 1100°C, accompanied by intermediate fine grinding. Full details of the preparation technique are given in the Appendix. All the compositions were less than 0.1 mm grain size particles composed of aggregates of less than 5μ crystals of forsterite and melilite, together with either diopside in the more siliceous charges or spinel in the less siliceous charges. Anorthite was identified in the more siliceous compositions and some of the less siliceous compositions. Monticellite has been identified in the X-ray patterns of the less siliceous charges but was destroyed during the runs. These starting assemblages were clearly metastable and represented incomplete recrystallization of the earliest phases to nucleate in the gels which appear to be dominantly melilite accompanied by some monticellite in gels of these compositions investigated at about 900°C.

The charges were placed in open platinum capsules and held at temperature in platinum-wound, resistance furnaces. Run temperatures are quoted relative to the liquidus of pure Li_2SiO_3, 1201°C, using a technique that yields either all liquid or all solid results in runs of a few hours duration at the melting points of silver, gold, and palladium in runs spaced less than 2°C apart. Lithium metasilicate and diopside both show about a 2°C melting interval. Temperature gradients within and between the twelve capsules in each assembly are less than $\pm$ 0.5°C at 1063°C. The temperatures quoted have been corrected for thermocouple drift where necessary, and temperatures relative to the liquidus in Li_2SiO_3 are given in tables 1 and 2. Precision of temperature control, using West Viscount proportional plus integral controllers, was better than $\pm$ 6μV (½°C) relative to the control couple emf. In the month long runs slow drift of the emf of the control couple, which was attached to the winding, resulted in an upward drift of the run temperature by 1 to 3°C as noted in the tables.

The small thermal gradients within and between capsules minimize the risks of generating assemblages stable on different sides of an equilibrium at opposite ends of a capsule or in different capsules within the same assembly. The small extent of temperature cycling greatly reduces the risk of persistently regenerating a metastable assemblage by devitrification at the solidus as the temperature falls. The long term upward

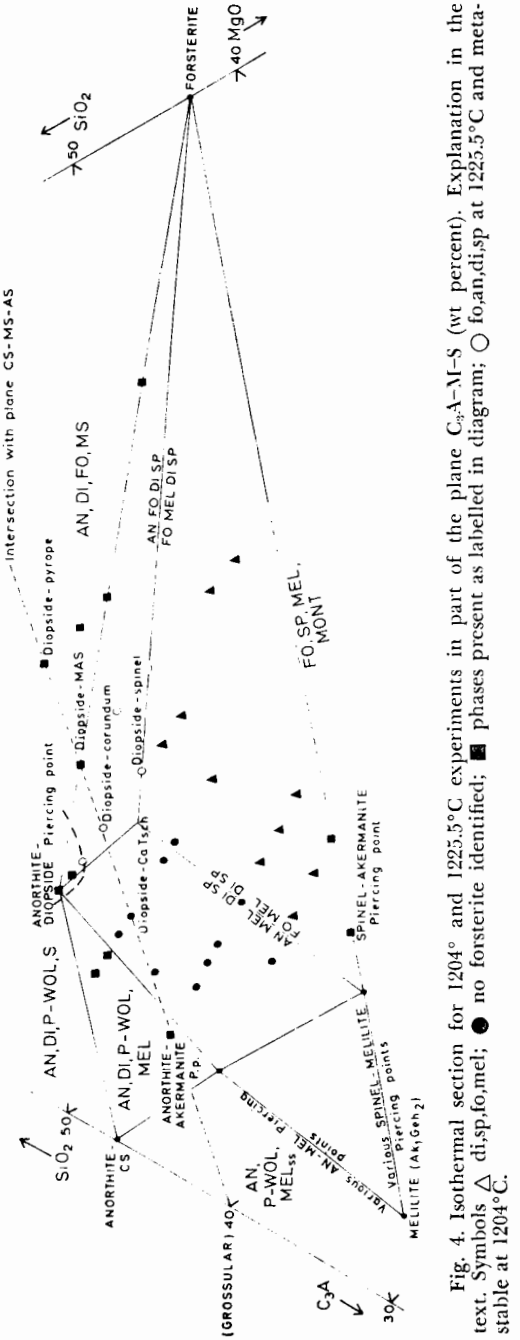

Fig. 4. Isothermal section for 1204° and 1225.5°C experiments in part of the plane C_3A–M–S (wt percent). Explanation in the text. Symbols △ di,sp,fo,mel; ● no forsterite identified; ■ phases present as labelled in diagram; ○ fo,an,di,sp at 1225.5°C and metastable at 1204°C.

TABLE 1

Details of operation of the two furnaces used in the present study

Run No.	Time	Pt:13%Rh-Pt recording thermocouple emf microvolts	Comments
4.c	3/4 hr	11335	Gold solid } 5.4°C interval. Required correction to thermo-
4.d	3/4 hr	11405	Gold liquid } couple temp. -1.5 ± 2.7°C.
4.l	2 hr	16089	Diopside liquid } 2.8°C interval. Required correction to
4.p	2-1/4 hr	16050	Diopside solid } thermocouple temp. -10.7 ± 1.4°C.
4.m	2-1/2 hr	18406	Palladium liquid } 1°C interval. Required correction to
4.q	2 hr	18395	Palladium solid } thermocouple temp. -15 ± 0.5°C.
4.x	2-1/2 hr	9864	Silver liquid } 5.8°C interval. Required correction to
4.y	2-1/2 hr	9789	Silver solid } thermocouple temp. +12.4 ± 2.9°C.
4.1	4-1/2 hr	13353	Lithium metasilicate solid } 4.0°C interval. Required
4.2	7 hr	13409	Lithium metasilicate liquid } correction to thermocouple temp. -10.4 ± 2.0°C.
4.3	37 days	13362-13403	Apparent 1209.9-1213.0; corrected to 1199.5-1202.6 ± 2.0°C.
4.4	29 days	13403-13419	Apparent 1213.0-1213.5; corrected to 1202.6-1204.1 ± 0.5°C.
4.5	2 hr	13358	Lithium metasilicate 50% liquid. Revised correction due to drift -9.4 ± 0.5°C.
4.6	29 days	13811-13825	Apparent 1242.4-1243.4; corrected to 1233.0-1234.7°C.
4.7	3-1/2 hr	13359	Lithium metasilicate liquid, trace primary crystals. Revised correction to thermocouple temp. -8.7°C.
4.8	30 days	13977-13998	Apparent 1254.3-1255.6; corrected to 1245.6-1246.9°C.
6.a	1/2 hr	11381	Gold liquid } 2.8°C interval. Correction to thermocouple
6.e	3/4 hr	11343	Gold solid } temp. -3.8 ± 1.4°C.
6.d	2 hr	18290	Palladium liquid } -0.3°C interval. Correction to thermo-
6.p	3 hr	18295	Palladium solid } couple temp. -7.2 ± 0.2°C.
6.l	6 hr	13295	Lithium metasilicate solid } 4.4°C interval. Correction
6.2	4-1/2 hr	13356	Lithium metasilicate liquid } to thermocouple temp. -6.5 ± 2.2°C.
6.3	37 days	13322-13368	Apparent 1207.2-1210.5; corrected 1200.7-1204.3 ± 1.8°C.
6.4	30 days	13354-13360	Apparent 1209.5-1210.0; corrected 1203.0-1203.8 ± 1.4°C.
6.5	2 hr	13251	Lithium metasilicate solid.
6.6	21 days	13709-13723	Apparent 1235.0-1236.0; corrected 1228.8-1230.5 ± 1.0°C.
6.7a	30 days	13704-13741	Apparent 1234.7-1237.3; corrected 1229.2-1232.2 ± 0.7°C.
6.7b	3-1/2 hr	13298	Lithium metasilicate 90% solid } 1.3°C interval. Correc-
6.8	3 hr	13317	Lithium metasilicate liquid } tion to thermocouple temp. -5.1 ± 0.7°C.
6.9	30 days	13817-13833	Apparent 1242.8-1244.0; corrected 1237.7-1239.7 ± 0.9°C.
6.10	24 days	13750-13781	Apparent 1238.0-1240.2; corrected 1233.7-1236.7 ± 1.0°C.
6.11	2 hr	13269	Lithium metasilicate solid } 2.0°C interval. Correction
6.12	2 hr	13296	Lithium metasilicate liquid } to thermocouple temp. -3.5 ± 1.0°C.
6.17	2 hr	13258	Lithium metasilicate liquid } Correction to thermo-
6.18	3 hr	13223	Lithium metasilicate 50% liquid } couple temp. -0.3 ± 1.3°C.
6.19	28 days	13561-13580	Apparent 1224.4-1225.8; corrected 1224.1-1225.5 ± 1.3°C.
6.20	3 hr	13208	Lithium metasilicate 50% liquid.

drift of 1 to 3° can, however, result in a particular equilibrium, for example, beginning of melting, being crossed late in the run, leaving insufficient time for the complete establishment of the new equilibrium, and hence yielding anomalously large numbers of coexisting phases. These technical problems are not restricted to the particular equipment used in this study.

Results obtained in the experiments are presented in table 4. Figure 4 contains an interpretation of the results obtained at temperatures close to 1200 to 1230°C where most of the compositions were converted substantially or completely to di + sp bearing assemblages from the an + fo + mel bearing starting materials. The presence of diopside and spinel was often established by microscopic examination at 250 to 500 magnifications and in all cases by X-ray studies (for example, fig. 5).

TABLE 2

Corrected and adopted terminating values of temperature in runs listed in table

Run no.	Corrected terminating temp., °C	Adopted terminating temp., °C
4.3	1202.6 ± 2.0	1204
6.4	1203.8 ± 1.4	1204
4.4	1204.1 ± 0.5	1204
6.3	1204.3 ± 1.8	1204
6.19	1225.5 ± 1.3	1225.5
6.6	1230.5 ± 1.0	1230.5
6.7a	1232.2 ± 0.7	1232
4.6	1234.7	1235
6.10	1236.7 ± 1.0	1237
6.9	1239.7 ± 0.9	1240
4.8	1246.9	1247

All temperatures relative to liquidus in Li_2SiO_3 at 1201°C.

The diopside + spinel assemblage persists in the presence of abundant glass at 1230 to 1235°C, and it is concluded in the light of these results that diopside + spinel is the more stable assemblage and is probably the equilibrium assemblage at temperatures above 1200°C and probably at lower temperatures also. Note that it has been found that *pure* akermanite does not coexist stably with either anorthite or spinel at this temperature, the maximum akermanite content of the melilite being about 80 percent. Results for a composition on the anorthite-akermanite join, 1M–C_3A–4S in table 4 and figure 4, show both pseudowollastonite *and* diopside to be present in small amounts (contrast de Wys and Foster, 1958). Results for a composition on the spinel-akermanite join, 2.5M–C_3A–3S, show forsterite to be present (fig. 4).

The beginning of melting $E_{an,\ mel,\ di,\ sp,\ l}$ is apparently encountered in a run whose temperature drifted from 1229.8 to 1230.6°C during the month. The temperature of this equilibrium is taken at 1230 ± 0.5°C. The other two solidus assemblages do not contain glass at this temperature. Therefore, $E_{fo,\ mel,\ di,\ sp,\ l}$ and $E_{an,\ fo,\ di,\ sp,\ l}$ must be encountered above 1230°C but below 1235°C, at which temperature all the compositions contain some glass, and the di + sp assemblage is no longer stable. $E_{an,\ fo,\ di,\ sp,\ l}$ must be encountered in the temperature range 1233.5 ± 1.5°C, whereas $E_{fo,\ mel,\ di,\ sp,\ l}$ must be encountered above 1231 ± 1.0°C.

Thus a temperature interval of 4 ± 2°C covers the whole of the di + sp + l bearing equilibria, a situation consistent with the composition surface of liquids in equilibrium with diopside and spinel ($L_{di,\ sp,\ l}$) being of very small extent, as would be expected if the pressure is close to that of $^4E^0_{an,\ fo,\ mel,\ di,\ sp,\ l}$ which may occur at less than atmospheric pressure.

A limited study was undertaken to account for the discrepancy between the results obtained in the present experiments and those previously obtained on similar chemical compositions by workers in other

laboratories. The most prominent difference lay in the physical state of the starting material, which in the case of the experiments reported here was a very fine grained crystalline product obtained from a gel whereas Schairer and co-workers used glass or glasses devitrified for various lengths of time at about 1050 to 1200°C. All starting materials probably reached temperature, in their respective runs, as anorthite + forsterite + melilite bearing charges because of the fast rate of devitrification of glasses in this system, but the grain size in the devitrified glasses was considerably greater than in the crystallized gel. The possibility that this increased grain size reduces the rate of conversion to the stable assemblage was tested by converting crystalline material of the 3M–C_3A–6S and 2.75M–C_3A–5S compositions (wt percent figs. in table 3) to glass, devitrifying it for 15 minutes at about 1150°C, when the products were diopside and forsterite, accompanied by identifiable anorthite and melilite in the second composition, and then holding it for 1 month at 1199°C, together with other capsules containing the crystallized gel starting material. The latter showed complete destruction of the anorthite + forsterite + melilite assemblage with growth of diopside + spinel, whereas the devitrified glass starting material showed no recognizable conversion to diopside + spinel under the same conditions.

DISCUSSION

The compositions of $L_{di,\ sp,\ l}$ as indicated by provisional isothermal sections (figs. 6 and 7) and the prediction of liquidus fields from published data (fig. 8) appear to lie very close to the plane C_3A–M–S, well within the tetrahedron an + mel + di + sp and beyond reasonable doubt within the external angle included by the planes fo + di + sp and an + di + sp projected beyond the di + sp join.

This situation in the quaternary system is analogous to that encountered in sapphirine-bearing equilibria in the ternary system MAS (Keith and Schairer, 1952). The four-phase tetrahedra an + di + sp + l and fo + di + sp + l cannot exist on the same side (with respect to temperature) of $^4E^1_{an,\ fo,\ di,\ sp,\ l}$ as the four-phase tetrahedra an + fo + sp + l and an + di + fo + l, both of which include large parts of the di + sp join which cannot, therefore, be solid under the same conditions. $^4E^2_{an,\ fo,\ di,\ l}$ and $^4E^2_{an,\ fo,\ sp,\ l}$ are known to occur at temperatures above 1233.5 up to 1278°C (O'Hara and Schairer, 1963) and 1320°C (Osborn and Tait, 1952) respectively. Consequently $^4E^2_{fo,\ di,\ sp,\ l}$ and $^4E^2_{an,\ di,\ sp,\ l}$ must be encountered below 1233.5°C. $^4E^1_{an,\ fo,\ di,\ sp,\ l}$ must be a distributary equilibrium in which both anorthite and forsterite must be in reaction relationship with the liquid (see flow sheet, fig. 9).

One di + sp mixture will melt to an + fo + l only in $^4E^1_{an,\ fo,\ di,\ sp,\ l}$. Upon fractional crystallization many liquids will approach the composition $L_{an,\ fo,\ di,\ sp,\ l}$ by fractionation of an + fo + sp or, more significantly, by fractionation of an + fo + di on their way down temperature toward silica-undersaturated compositions from the thermal divide which lies close to the plane of critical undersaturation of silica

TABLE 3

Details of composition in the plane C_3A-M-S utilized in the present study

Moles M per C_3A	Moles S per C_3A	Weight percentages				Comments
		SiO_2	MgO	CaO	Al_2O_3	
1	3	36.73	8.21	34.28	20.78	
2.5	3	32.70	18.28	30.52	18.50	$2MA + 3C_2MS_2$ Sp-Ak join
1	3.5	40.38	7.74	32.30	19.58	
2	3.5	37.48	14.37	29.98	18.17	
2.5	3.5	36.18	17.34	28.94	17.54	
3	3.5	34.97	20.11	27.97	16.95	
3.5	3.5	33.83	22.70	27.07	16.40	$2MA + 3C_2MS_2 + M_2S$ Sp-Ak-Fo plane
1	4	43.63	7.32	30.54	18.51	$CAS_2 + C_2MS_2$ An-Ak join
1.25	4	42.85	8.98	29.99	18.18	
1.5	4	42.09	10.59	29.46	17.86	
1.75	4	41.36	12.14	28.95	17.55	
2	4	40.66	13.64	28.46	17.25	$6C_2MS_2 \cdot 2C_2AS + 5CAS_2 + 4M_2S$; $Ak_{75}Geh_{25}$-An-Fo plane
2.5	4	39.32	16.49	27.52	16.68	
3	4	38.06	19.15	26.64	16.15	
3.5	4	36.88	21.65	25.82	15.65	
4	4	35.78	24.00	25.04	15.18	
1.5	4.5	44.99	10.06	27.99	16.96	En-Gross join
1.25	5	48.38	8.11	27.09	16.42	
1.5	5	47.60	9.58	26.66	16.16	$2CAS_2 + 2CMS_2 + C_2MS_2$ An-Ak-Di plane
1.75	5	46.86	11.00	26.24	15.90	
2	5	46.13	12.38	25.83	15.66	$2CMS_2 + CAS$ Di-CaTsch join
2.75	5	44.08	16.27	24.69	14.96	
3	5	43.44	17.49	24.33	14.74	
4	5	41.05	22.03	22.99	13.93	$6C_2MS_2 \cdot 2C_2AS + 5CAS_2 + 11M_2S$; $Ak_{75}Geh_{25}$-An-Fo plane
2	6	50.68	11.33	23.65	14.33	$2CMS_2 + CAS_2$ An-Di join
2.25	6	49.97	12.57	23.32	14.13	
2.5	6	49.28	13.78	23.00	13.94	
3	6	47.96	16.09	22.38	13.57	$3CMS_2 + A$ Di-Al_2O_3 join
4	6	45.52	20.36	21.24	12.88	$3CMS_2 + MA$ Di-Sp join
4.5	6	44.39	22.34	20.72	12.56	
5	6	43.32	24.22	20.22	12.25	
4	7	49.36	18.92	19.75	11.97	$3CMS_2 + MAS$ Di-MAS join; $2CMS_2 + CAS_2 + M_2S$ Di-An-Fo plane
5	7	47.13	22.59	18.85	11.43	
6	7	45.10	25.93	18.04	10.93	$3CMS_2 + MA + M_2S$ Di-Sp-Fo plane
8	7	41.51	31.83	16.60	10.06	$6C_2MS_2 \cdot 2C_2AS + 5CAS_2 + 25M_2S$; $Ak_{75}Geh_{25}$-An-Fo plane
9	7	39.92	34.43	15.97	9.68	
6	9	51.36	22.97	15.98	9.68	$3CMS_2 + M_3AS_2$ Di-pyrope join
7	9	49.47	25.81	15.39	9.33	
7.5	9	48.57	27.16	15.11	9.16	
8	9	47.71	28.45	14.84	9.00	$2CMS_2 + CAS_2 + 3M_2S$ Di-An-Fo plane
9	9	46.07	30.91	14.33	8.69	
20	15	45.57	40.77	8.51	5.16	$2CMS_2 + CAS_2 + 9M_2S$ Di-An-Fo plane
22	15	43.79	43.09	8.17	4.95	$3CMS_2 + MA + 9M_2S$ Di-Sp-Fo plane
24	15	42.14	45.23	7.87	4.77	
27	15	39.88	48.16	7.45	4.51	

TABLE 4

Results of quenching experiments

Temp., °C	Time, days	Run	Moles M per C_3A	Moles S per C_3A	Optical	X-ray
1204	37	4.3	2.75	5	di,mel	di,sp,mel,(? no fo)
			4	5	di,(sp),mel	di,sp,mel,fo
			2	6	di,an,?(gl)	di,an
			2.25	6		di,an
			2.5	6	di,an	di,an,(fo)
			3	6	di,an	di,sp,an,fo
			4	6	di,an	di,sp,an,mel,fo
			4.5	6	di,sp	di,sp,fo,(? mel)
			5	6	di,sp,mel	di,sp,mel,fo
1204	30	6.4	2	3.5	di,sp,an,mel	di,sp,(an),mel
			1.5	4	di,(sp),an,mel	di,sp,an,mel
			1.75	4	di,sp,an,mel	di,sp,an,mel
			2	4	di,sp,an,mel	di,sp,an,mel
			3	4	di,sp,mel	di,sp,mel,(fo)
1204	37	6.3	20	15		di,an,fo
			27	15		sp,fo,mel,mont ? metastable
1204	29	4.4	1	4	(di),an,mel,(pwol)	(di),an,mel
			4	4		(di),sp,mel,fo
			1.25	5	di,an	di,an,mel,wol
			1.5	5	di,an	di,an,mel,?wol
			1.75	5	di,an,mel	di,an,mel
			2	5	di,sp,an	di,sp,an,mel
1225.5	28	6.19	1.5	4.5	di,(sp),an,mel	di,(sp?),an,mel
			1.75	5	an,di,mel,(?sp)	an,di,mel,(?sp)
			2	5	an,di,mel,(sp)	an,di,mel,(sp)
			2.75	5	di,sp,mel	di,sp,mel
			3	5	di,sp,mel	di,sp,mel
			2.25	6	an,di	an,di
			4	6	di,fo,sp	di,fo,sp*
			5	6		di,sp,fo,(mel)
1230.5	21	6.6	2.5	3.5	di,sp,mel	di,sp,mel,(fo)
			3	3.5	di,sp,mel,?fo	di,sp,mel,fo
			3.5	3.5	sp,mel,?fo	sp,mel,fo
			1	4	an,mel,di	an,mel
			1.25	4	di,sp,an,mel,gl	(di),an,mel
			2.5	4	di,sp,mel,fr	di,sp,mel,(fo)
			3.5	4	di,sp,mel	di,sp,mel,fo
			4	4	di,sp,mel,fo	(di),sp,mel,fo
1232	30	6.7a	1	3.5	sp,an,mel,gl	sp,an,mel
			2	3.5	di,sp,mel,(an?),gl	di,sp,mel
			1.5	4	di,sp,an,mel,gl	di,sp,an,mel
			1.75	4	di,sp,an,mel,gl	di,sp,an,mel
			2	4	di,sp,mel,gl	di,sp,mel
			1.25	5	di,an,(gl)	di,an
			1.5	5	di,an,mel,(gl)	di,an,mel
			1.75	5	di,an,(mel),(gl)	di,an,(mel)
			2	5	di,(sp),(an),gl	di,an
			2.75	5	di,sp,fo,mel,(gl)	di,sp,mel,fo

TABLE 4 (continued)

Temp., °C	Time, days	Run	Moles M per C_3A	Moles S per C_3A	Optical	X-ray
1235	29	4.6	2.5	6	di,an	di,an,fo
			3	6	di,an,(gl)	di,an,fo
			4	6	(di),sp,fo,gl	di,sp,fo
			4	7	di,an,fo	di,an,fo
			5	7	di,(sp),an,fo	di,(sp),an,fo
			6	7	di,sp,an,fo,gl	di,sp,an,fo
			6	9	di,an,fo	di,an,fo,?MS
			8	9	di,an,fo	di,an,fo
			9	9	di,an,fo,(?sp),(gl)	di,an,fo
1237	24	6.10	2.5	3.5	sp,mel,fo,gl	
			2	4	sp,mel,fo,gl	
			2.5	4	sp,mel,fo,gl	sp,mel,(fo)
			3	4	sp,mel,fo,gl	
			3.5	4	sp,mel,fo,gl	
			2	5	di,(an),gl	di,(an)
			2.75	5	di,fo,gl	
			3	5	sp,fo,(?mel),gl	
			4	5	sp,fo,mel,gl	
			4	6	di,an,fo,gl	di,an,fo
			4.5	6	di,fo,gl,(?an)	
			5	6	di,fo,gl	
1240	30	6.9	2	3.5	sp,mel,(fo),gl	
			2.5	3.5	sp,mel,fo,gl	
			1.5	4	sp,mel,gl	
			1.75	4	sp,mel,gl	
			2	4	sp,mel,(fo),gl	
			2.5	4	sp,mel,fo,gl	
			1.75	5	di,an,gl	di,(an)
			2	5	di,an,(fo),gl	di
			2.75	5	(di),fo,gl	
			3	6	di,an,(fo),gl	di,fo,(an)
			4	6	di,an,fo,gl	
			6	7	di,an,fo,gl	di,(an),fo
1247	30	4.8	2	3.5	sp,mel,(fo),gl	
			2.5	3.5	sp,mel,(fo),gl	sp,mel
			1.5	4	sp,mel,gl	
			2	4	sp,mel,(fo),gl	
			2.5	4	sp,mel,fo,gl	
			3.5	4	sp,mel,fo,(gl)	sp,mel,(fo)
			1.75	5	di,an,gl	di,(an)
			2	5	di,(an),(fo),gl	di
			2.75	5	fo,gl	
			2.5	6	di,an,(?fo)	di,an,?fo
			3	6	di,an,?fo	di,an,fo
			4	6	fo,gl	

? = identification questionable, based on one or two crystals only.
() = small amounts only.
fr = fritted.
*Recrystallized at 1225.5°C, metastable at 1204°C.

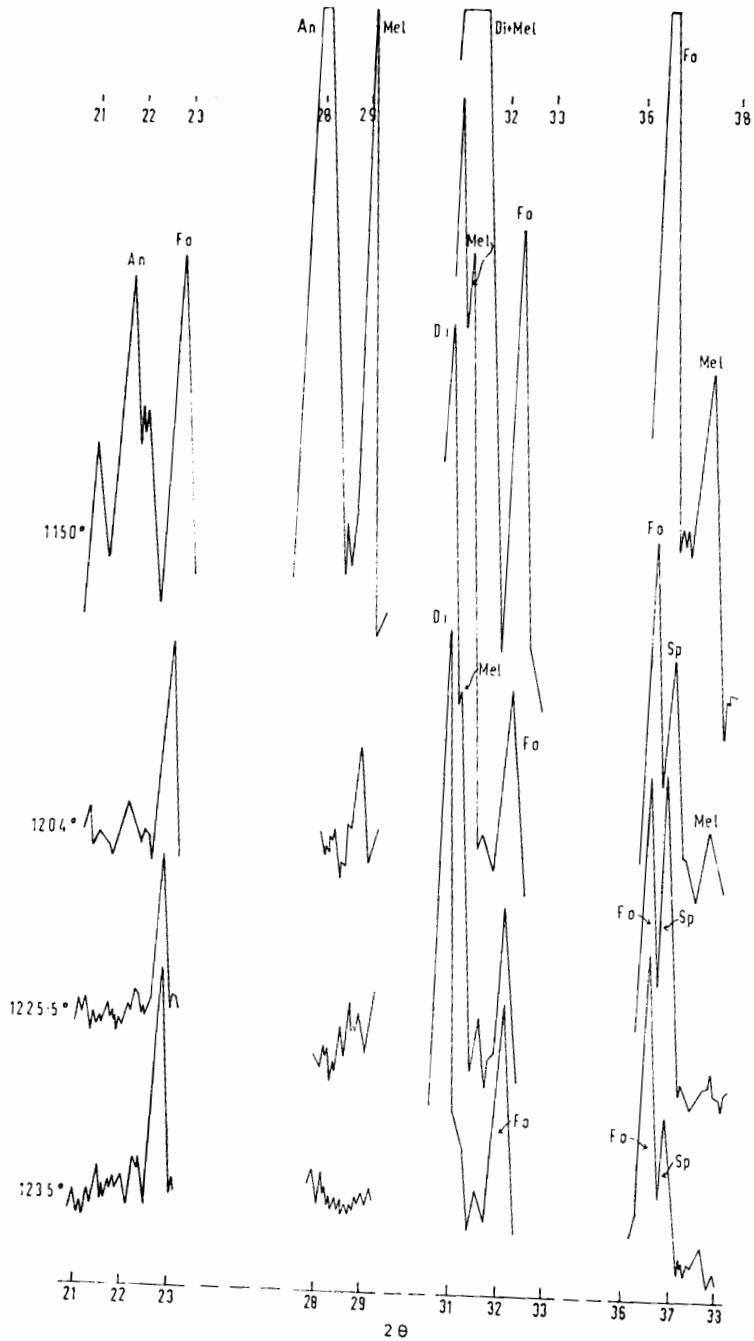
An
Mel
Di+Mel
Fo
21
22
23
28
29
32
33
36
38
An
Fo
Mel
Di
Mel
1150°
Fo
Di
Sp
Mel
Fo
1204°
Mel
Fo
Sp
1225·5°
Fo
Fo
Sp
1235°
21
22
23
28
29
31
32
33
36
37
38
2θ

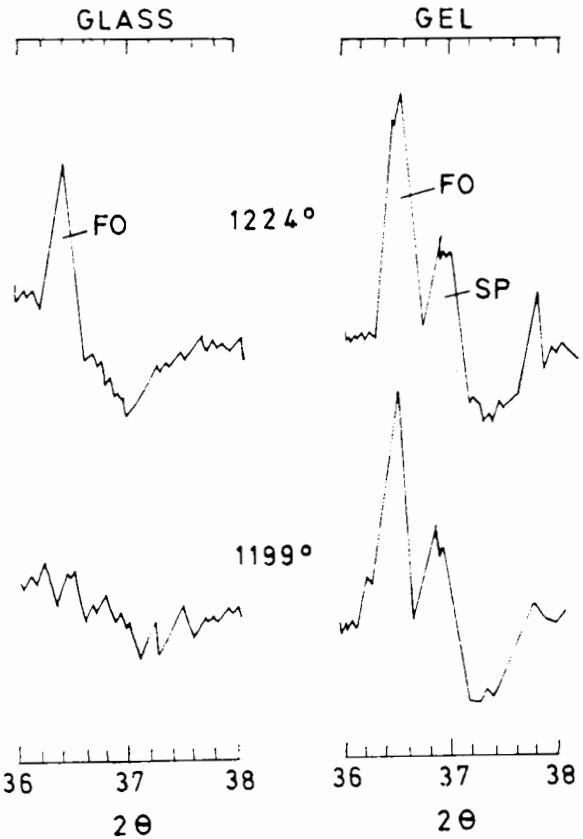

Fig. 5A. Parts of the X-ray patterns obtained from starting material of the 4M–C_3A–6S composition, 1150°C, and products of about 1 month runs at 1204°C, 1225.5°C, and 1235°C. Note the reduction of the anorthite and melilite intensities and the increase in spinel intensity with rising temperature. The run at 1235°C was partially melted. Note the increased intensity of the forsterite peak relative to spinel near 36.5° 2θ ($CuK\alpha$ radiation). The run at 1237°C, not illustrated, shows the total disappearance of spinel and the reappearance of recognizable anorthite.

Fig. 5B. Tracings from X-ray diffractometer charts showing the failure of a devitrified glass charges of composition 3M–C_3A–6S to nucleate (1) Fo and spinel at 1199° and (2) spinel at 1224°. At both temperatures the gel gives an assemblage of An, Di, Fo, Sp. The experiments from which these data are obtained are not listed in the tables.

CAS_2–M_2S–CMS_2, anorthite–forsterite–pure diopside (O'Hara and Schairer, 1963, p. 111). The extension of this thermal divide into more complex systems is an important factor in basalt petrogenesis at low pressures (Yoder and Tilley, 1962; Schairer and Yoder, 1964). At $^4E^1_{an,\ fo,\ di,\ sp,\ 1}$ the fractionating liquids which are strongly undersaturated in silica cease to precipitate *both* anorthite and forsterite and continue their fractional crystallization by precipitation of di + sp only in $^4E^3_{di,\ sp,\ 1}$ for a short temperature interval before encountering $^4E^2_{mel,\ di,\ sp,\ 1}$ where melilite appears as a precipitating phase (see fig. 9). The liquid composition

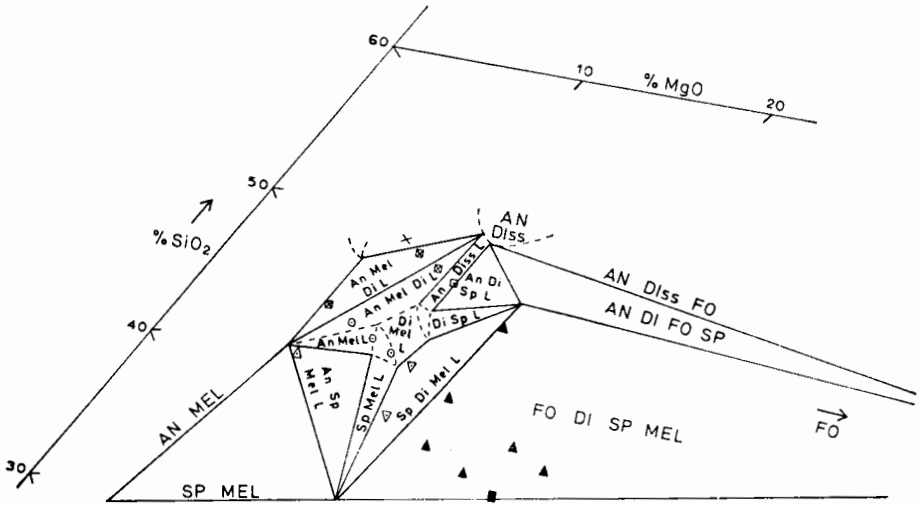

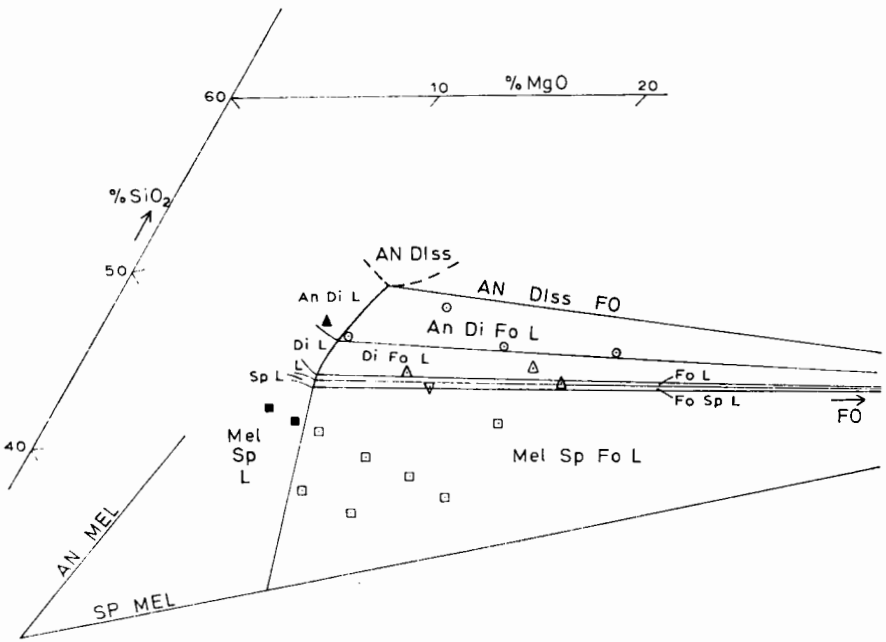

Figs. 6 and 7. Provisional "isothermal" sections for part of the plane C_3A–M–S at temperatures of "1230.5 to 1232°C" and "1237 to 1240°C" to illustrate the relationship between the liquid compositions in equilibrium with diopside + spinel and the subsolidus tetrahedra. Four-sided phase areas result whenever two phases lie to one side of the section and two to the other.

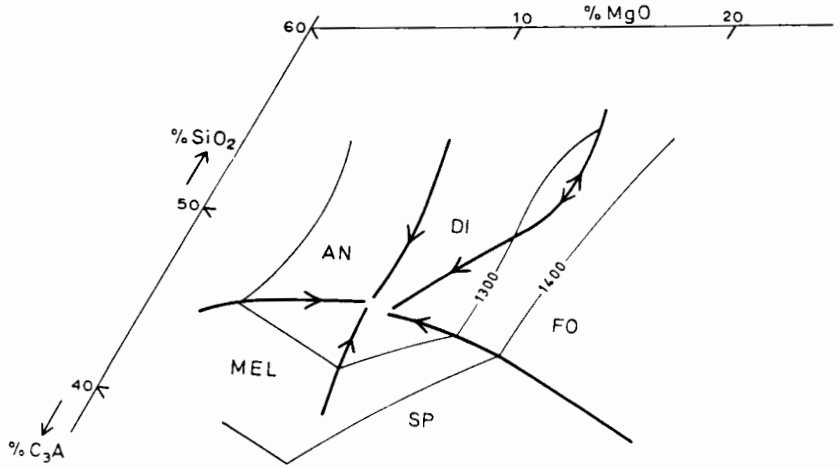

Fig. 8. Liquidus fields in part of the section C_3A–M–S predicted from published data referred to in the text by methods similar to those described by Chinner and Schairer (1962).

then proceeds to ${}^4E^1_{an,\ mel,\ di,\ sp,\ l}$ where anorthite reappears, and the remaining liquid freezes in the eutectic relationship.

${}^4E^2_{an,\ di,\ sp,\ l}$ and ${}^4E^2_{fo,\ di,\ sp,\ l}$ which run down temperature from ${}^4E^2_{an,\ fo,\ di,\ sp,\ l}$ to ${}^4E^1_{an,\ mel,\ di,\ sp,\ l}$ and ${}^4E^1_{fo,\ mel,\ di,\ sp,\ l}$ respectively (fig. 9) must involve the resorbtion of anorthite and forsterite, respectively.

${}^4E^2_{fo,\ di,\ sp,\ l}$ runs down temperature to ${}^4E^1_{fo,\ mel,\ di,\ sp,\ l}$. Composition $L_{fo,\ mel,\ di,\ sp,\ l}$ falls outside the tetrahedron fo + mel + di + sp in such a way that the four-phase tetrahedra fo + di + sp + l, fo + mel + sp + l, and fo + mel + di + l at a temperature fractionally above ${}^4E^1_{fo,\ mel,\ di,\ sp,\ l}$ all include parts of the composition plane di + sp + mel which must become solid in the univariant equilibrium. Consequently ${}^4E^2_{fo,\ di,\ sp,\ l}$, ${}^4E^2_{fo,\ mel,\ sp,\ l}$, and ${}^4E^2_{fo,\ mel,\ di,\ l}$ must all exist at temperatures above ${}^4E^1_{fo,\ mel,\ di,\ sp,\ l}$.

${}^4E^1_{fo,\ mel,\ di,\ sp,\ l}$ is, therefore, a simple reaction equilibrium in which forsterite is resorbed and would cease to precipitate during fractional crystallization.

${}^4E^2_{mel,\ di,\ sp,\ l}$ must run down temperature from ${}^4E^1_{fo,\ mel,\ di,\ sp,\ l}$ to ${}^4E^1_{an,\ mel,\ di,\ sp,\ l}$ where it meets ${}^4E^2_{an,\ di,\ sp,\ l}$, ${}^4E^2_{an,\ mel,\ di,\ l}$, and ${}^4E^2_{an,\ mel,\ sp,\ l}$ all of which have run down temperature into ${}^4E^1_{an,\ mel,\ di,\ sp,\ l}$, an eutectic (see fig. 9).

ISOTHERMAL SECTIONS

Attempts have been made to draw isothermal sections for the region of the plane C_3A–M–S investigated. The compositions of $L_{an,\ di,\ fo,\ sp,\ l}$, $L_{fo,\ mel,\ di,\ sp,\ l}$, and $L_{an,\ mel,\ di,\ sp,\ l}$ lie very close to the plane, but their positions relative to the plane are not precisely known. The five liquidus fields of an, di, fo, sp, and mel in this plane converge almost to a point, and there are four possible choices for the three piercing points of loci of liquids in divariant (isobaric univariant) equilibria. The relative tem-

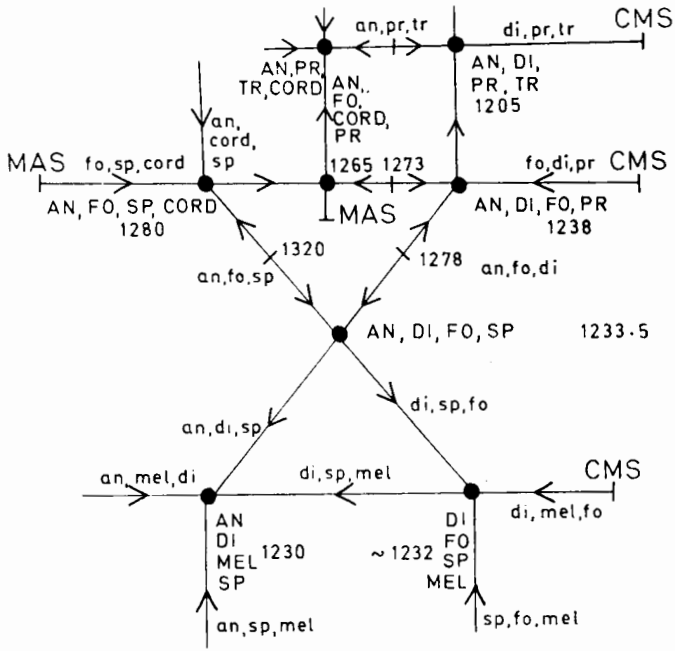

Fig. 9. Partial flow sheet for the system CMAS incorporating the diopside + spinel bearing equilibria and showing their relationship to cordierite (cord), protoenstatite (pr), and tridymite (tr) bearing equilibria.

peratures of the three piercing points and the three univariant (isobaric invariant equilibria) are not known, and numerous alternative possibilities exist. An analysis has shown that 42 figures are necessary to illustrate all possible sequences of isothermal sections between 1228°C in the solidus and a temperature of about 1250°C, which are consistent with the experimental data, and there are 65 possible sequences of the isothermal sections. A diagrammatic analysis is presented in figure 10, whereas figure 11 presents the four possible forms of the liquidus, one of which is consistent with each of the quadrants of figure 10. In each of the four liquidus diagrams dotted lines indicate the self- projections of the loci of liquids in divariant (isobaric univariant) equilibria, separating each liquidus field into subfields according to the nature of the second crystalline phase to appear in the compositions concerned. With the aid of figures 10 and 11, the reader can construct the 42 diagrams. Those indicated by heavy type in figure 10 appear in more than one of the alternative sequences (no. 3 appears in 44 of the 65 sequences for example). It is hoped to narrow down the possibilities by further observations.

EXPERIMENTAL SIGNIFICANCE OF THE NEW RESULTS

Although the range of liquid compositions in equilibrium with diopside and spinel in the system C–M–A–S is so small, the range of bulk

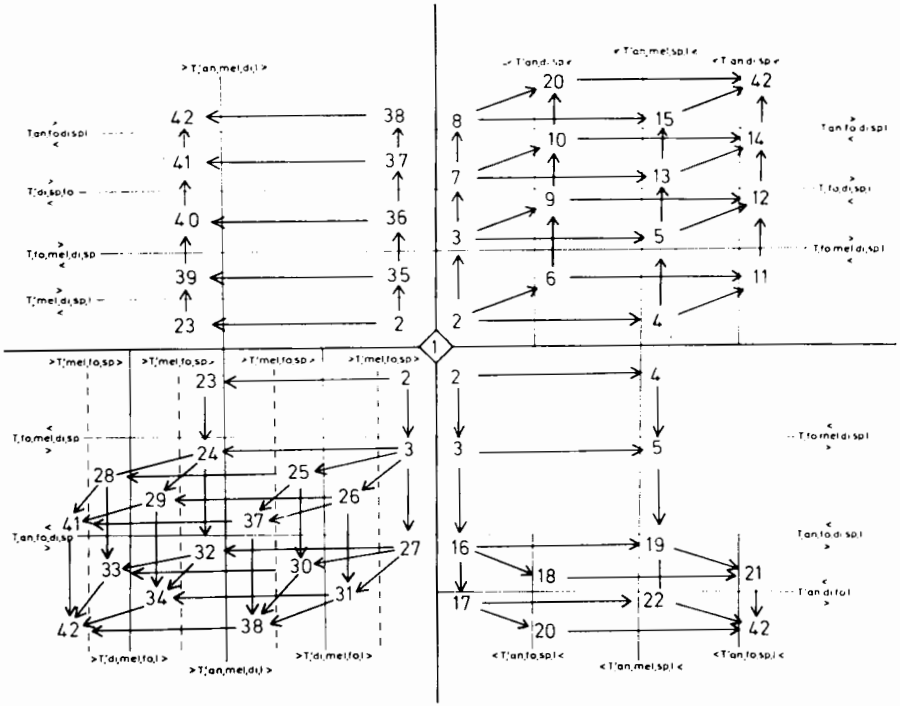

Fig. 10. Scheme of isothermal sections and possible sequences between them which are consistent with available data for part of the section C_3A–M–S. Each quadrant of the figure corresponds with the equivalent quadrant of the alternative liquidus diagrams in figure 11. Temperature rises away from the central part of the figure, and the light ruled lines divide the figure into boxes. Crossing one of these lines implies a change of temperature across that appropriate to one of the isobaric invariant equilibria (for example, $T_{fo,mel,di,sp,l}$) or one of the piercing points of isobaric univariant equilibria in the section C_3A–M–S (labelled for example $T^1_{an,di,fo,l}$). The numerous possibilities arise because the relative order of the temperatures of the two isobaric invariant equilibria and the nine possible piercing points shown in figure 11 are not known. In each quadrant a double ruled line separates two parallel sets of possibilities.

compositions which develop di + sp bearing subsolidus assemblages, and, therefore, encounter the di + sp + l equilibria, is very large. Consequently relationships involving di + sp will be encountered over substantial parts of many pseudobinary joins and pseudoternary sections of the system, and revisions will be necessary in a number of published diagrams (for example, Chinner and Schairer, 1962, figs. 2, 4, 5, 7; de Neufville and Schairer, 1962, figs. 1, 2; O'Hara and Schairer, 1963, figs. 32, 35, 36; Schairer and Kushiro, 1965, fig. 21; and Muan and Osborn, 1965, fig. 120).

The diopside composition that coexists with spinel must lie to the silica-poor and lime + alumina-rich side of that which coexists with anorthite and forsterite at the thermal maximum on $^4E^2_{an,\ fo,\ di,\ l}$. That diopside is itself known to be silica-poor with respect to the composition plane CMS_2–CAS_2–M_2S (O'Hara and Schairer, 1963) hence the diopside that coexists with spinel must lie outside the sub-system anorthite +

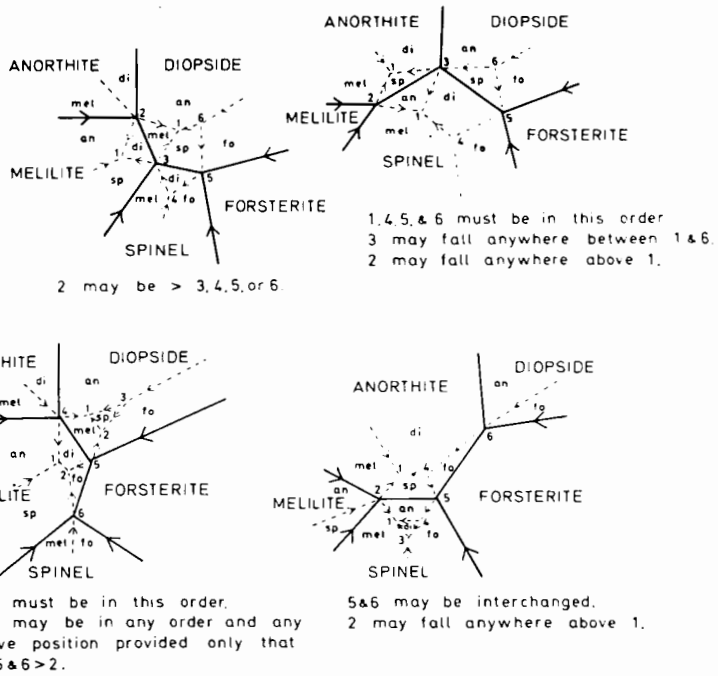

Fig. 11. Four alternative schematic possibilities for the form of the liquidus fields in part of the section C_3A–M–S, showing nine possible piercing points of loci of liquids in isobaric univariant equilibria. Within each liquidus field broken lines indicate the nature of the second crystalline phase to appear on cooling. These lines are projections into the plane C_3A–M–S toward the liquidus phase composition of the loci of liquids in appropriate isobaric univariant and invariant equilibria. The nature of the second crystalline phase to precipitate is indicated in each area. In each figure the relative temperatures of the three piercing points and three isobaric invariant equilibria are numbered 1 to 6 in order of ascending temperature as far as known, subject to qualifications under each quadrant. The four possibilities correspond to the equivalent four quadrants of figure 10, respectively. Arrows indicate directions of falling temperature where known.

forsterite + diopside + silica. Thus Osborn and Tait's (1952) conclusion that diopside + spinel is not stable at the solidus in that subsystem of the system CMAS remains valid and is unaffected by the results reported here.

GEOLOGICAL APPLICATIONS

The reaction relationship between diopside and silica-poor liquid in $^{4}E^{1}_{an,\ fo,\ di,\ mel,\ l}$ which was discussed by Chinner and Schairer (1962) no longer appears in the revised flow sheet. Instead, reaction relationships between forsterite or anorthite and very silica-poor liquids are reported. Forsterite-liquid reaction relationships in silica-poor liquids have been reported before (Schairer and Yoder, 1964), and forsterite-liquid reaction relationships to produce diopside are now known from silica over-saturated liquids in the system C–M–S (Boyd and Schairer, 1964) in $^{3}E^{2}_{fo,\ di,\ l}$, and such reaction relationships persist into the sys-

tem CMAS in $^{4}E^{3}_{fo,\ di,\ l}$ where the liquid compositions may be inferred to be both silica over-saturated and silica under-saturated (O'Hara and Schairer, 1963, fig. 31, which displays this reaction relationship in the diopside-rich region). A reaction relationship between forsterite and silica-poor liquids in the system CMAS has not previously been reported, but like its counterpart in the system nepheline–larnite–forsterite–silica (Schairer and Yoder, 1964), it is likely to extend into more complex systems and may play an important part in the genesis of olivine-free silica-poor rocks such as the nephelinites and melilitites (see below).

The anorthite-silica poor liquid reaction relationship to yield diopside + spinel appears to be unique, no calcic plagioclase-liquid reaction relationship resulting in the disappearance of plagioclase on fractionation having been reported from any anhydrous system before. How far it extends into the more complex systems is unknown, but it may prove to be important in explaining the genesis of plagioclase-free derivatives, such as the nephelinites and melilitites from plagioclase-precipitating parental magmas (see below)

The influence of pressure upon the diopside + spinel equilibria is profound. Diopside + spinel is probably stable to well above 45 kb (MacGregor, 1965), and the diopside + spinel + liquid equilibria extend through wide ranges of temperature and are encountered by much wider ranges of compositions in the system C–M–A–S and C–M–A–S–H_2O at high pressures (Kushiro and Yoder, 1966; Yoder and Chinner, 1960). It cannot be doubted that the effect of the first few hundred bars pressure will be to enlarge the temperature range of the di + sp + l equilibrium and the range of liquid compositions concerned in the system C–M–A–S, thus enhancing the effects obtainable by fractional crystallization as described above without changing the fundamental character of the equilibria concerned.

Certain compositions on the diopside–Ca Tschermak's molecule join which yielded homogeneous diopside solid solutions on devitrification which persisted in short experiments (de Neufville and Schairer, 1962) were shown to recrystallize to a less aluminous diopside + anorthite + forsterite + melilite on longer heating (O'Hara and Schairer, 1963), but this assemblage is itself metastable and should, on still longer heating, react to yield the diopside + spinel + anorthite + melilite assemblage in these particular compositions. The system CMAS has already yielded an example of the rapid formation of a metastable phase (diopside) by devitrification of glass, which only slowly recrystallizes to the stable assemblages. The present results show an instance of formation of a metastable 3-phase assemblage, at the expense of diopside crystallization despite the fact that in other parts of the system diopside forms so readily. This is a two-stage conversion process in which one metastable assemblage changes to another, and then the second changes to the stable assemblage.

If the relationship described above from the silica-poor part of the system CMAS were a fair representation of the situation in natural silica-poor basic igenous rocks, it would be expected that perfect fractional

crystallization of liquids lying just to the silica-poor side of the thermal divide olivine + plagioclase + diopside would yield accumulate sequences containing diopside + spinel rock with or without melilite, and lavas in which diopside + spinel and perhaps also melilite phenocrysts were embedded in a plagioclase+ olivine + melilite groundmass obtained as a metastable devitrification product. In practice none of these assemblages are significant in natural silica-poor basic rocks. The most important additional components present in the natural rocks are Na_2O and FeO. The addition of either will lower liquidus temperatures and, therefore, might be expected to increase the extent of the diopside + spinel + liquid region initially and to enhance the potential effect of these equilibria upon the evolution of natural magmas. Substitution of FeO for MgO in the ratios observed in natural rocks does not produce any new iron-rich phases in equilibria of the type under discussion. Addition of Na_2O to the system does, however, in the form of the silica-poor phase nepheline which is known to enter into equilibria with melilite, plagioclase, olivine, and diopside. The absence of diopside + spinel and plagioclase + melilite + olivine assemblages from natural silica-poor lavas may be ascribed to the presence of substantial amounts of Na_2O.

It is instructive to consider the likely effect of Na_2O upon the equilibria described here, using available information for the system CMAS and the sections nepheline–larnite–forsterite–silica and nepheline–diopside–anorthite of the system Na_2O–CMAS, although it is difficult to envisage the relationships in the customary geometrical terms.

Figure 12 is a modified flow sheet for part of the system CMAS, showing all the trivariant, divariant (isobaric univariant), and univariant (isobaric invariant) equilibria involving diopside and liquid *but no other equilibria*. Each trivariant equilibrium in this skeleton figure is represented by an area labelled in figure 14, a composite of figures 12 and 13, with the name of the phase X, coexisting with diopside and liquid in ${}^4E^3_{di,\ X,\ l}$. Senses of falling temperature on the lines representing the loci of liquids in divariant equilibria, such as ${}^4E^2_{an,\ fo,\ di,\ l}$, are shown, in figure 14 and the temperatures of thermal divides and of univariant equilibria are shown where known.

When small amounts of Na_2O are added to the system each point representing a univariant equilibrium must give rise to a divariant equilibrium in the five component system such as ${}^5E^2_{di,\ fo,\ plag,\ pr,\ l}$ generated from ${}^4E^1_{di,\ fo,\ an,\ pr,\ l}$ (plag = plagioclase, pr = protoenstatite). Any section of the five-component system will reveal pseudo-univariant (isobaric pseudo-invariant) equilibria which are the piercing points of ${}^5E^2$ in that particular section.

Schairer and Yoder (1964) have presented a flow sheet for the section nepheline–larnite–forsterite–silica in which a number of such piercing points are shown, linked by lines which may be regarded as the intersection of the section with surfaces that are the loci of liquids in ${}^5E^3$.

Figure 13 is taken with modification and relettering from Schairer and Yoder (1964) and shows the pseudo-flow sheet of equilibria involving diopside and liquid in that section. Points Q, R. S are pseudo-univariant and represent the piercing points of,

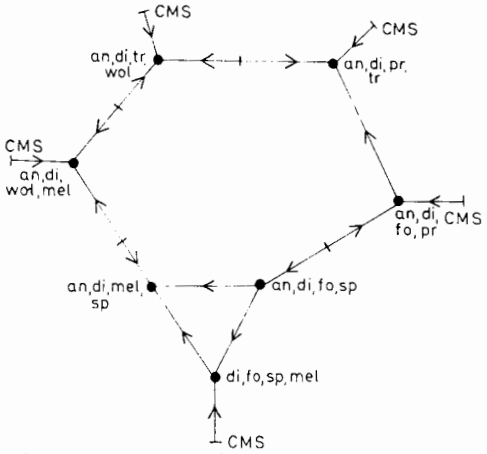

Fig. 12 Partial flow sheet of diopside bearing equilibria in the system CMAS. Explanation in the text.

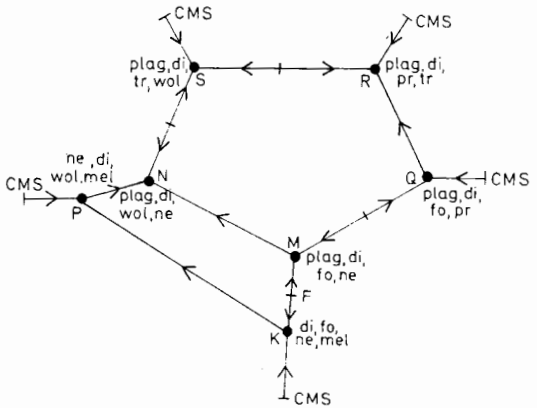

Fig. 13. Partial flow sheet of diopside-bearing equilibria in the section nepheline–larnite–forsterite–silica. Explanation in the text.

respectively, $^5E^2_{di,\ ol,\ pr,\ plag,\ l}$, $^5E^2_{di,\ pr,\ plag,\ tr,\ l}$, and $^5E^2_{di,\ plag,\ tr,\ wol,\ l}$ (tr = tridymite, wol = wollastonite), which derive directly from $^4E^1_{di,\ fo,\ pr,\ an,\ l}$, $^4E^1_{di,\ pr,\ an,\ tr,\ l}$, and $^4E^1_{di,\ an,\ wol,\ tr,\ l}$ of the system CMAS (fig. 12). The other points K, M, N, P are pseudo-univariant and represent piercing points of, respectively, $^5E^2_{di,\ ne,\ mel,\ fo,\ l}$, $^5E^2_{di,\ ne,\ plag,\ fo,\ l}$, $^5E^2_{di,\ ne,\ plag,\ wol,\ l}$, and $^5E^2_{di,\ wol,\ mel,\ l}$ which do not emerge directly from any of the $^4E^1$ of CMAS (fig. 12). Transition from figure 12 to figure 13 can only be effected via a number of univariant equilibria of the five-component system whose liquid compositions fall between the system CMAS and the section nepheline–larnite–forsterite–silica.

Figure 14 superimposes figures 12 and 13 in such a way that the reader may visualize the relationships in perspective, the flow sheet of figure 12 appearing close to the observer (solid lines and shaded circles) while that of figure 13 is seen behind it (dashed lines and small open circles), removed from the observer along an axis representing increase of Na_2O. Heavy lines represent $^5E^2$ generated from the $^4E^1$ of figure 12 and piercing the section of figure 13 at the small circles. The reader will identify at the top right of the figure the three $^5E^2$ that run directly from CMAS to pierce at Q, R, and S, as described above.

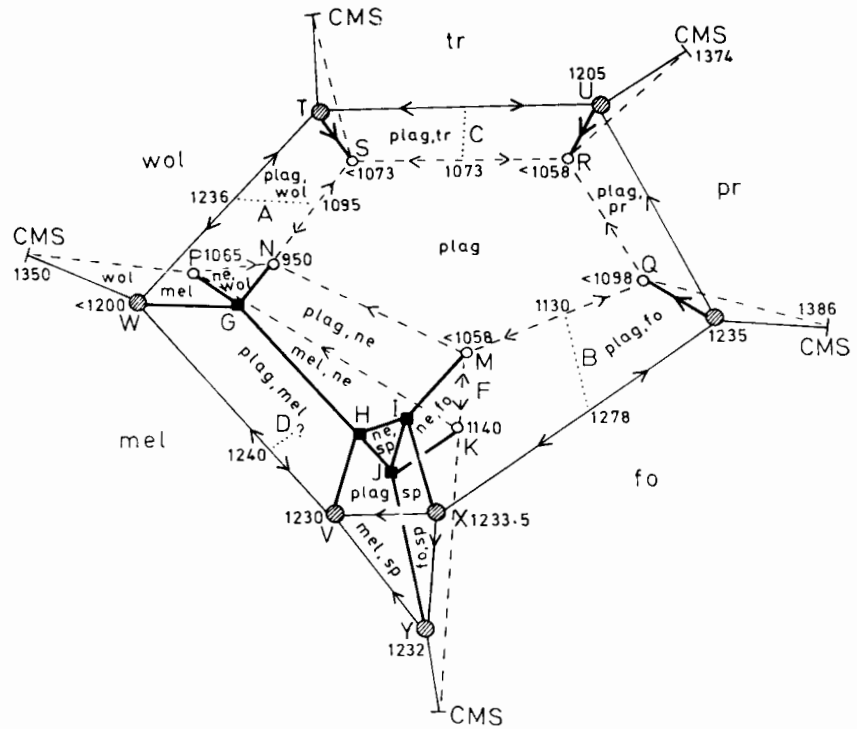

Fig. 14. Perspective of flow model for diopside-bearing equilibria of part of the system Na_2O–CMAS. Explanation in the text.

The central core of the figure is a volume labelled "plag", representing equilibrium between plagioclase, diopside, and liquid (all equilibria involve diopside and liquid, and these phases are, therefore, omitted from the labelling). This central core is bounded by several other volumes (for example, mel, sp, fo, pr, tr, wol) which abut against it in polygonal facets. These facets, seen in perspective in figure 14, represent the loci of liquids in equilibrium with diopside + plagioclase + one of wol, mel, sp, fo, pr, tr, and are labelled with the two solid phases other than diopside. Facet RSTU, for example, represents the locus of liquids on $^5E^3_{di,\ plag,\ tr,\ l}$.

In the lower left hand part of the figure relationships are more complicated. The plagioclase + diopside + liquid volume abuts against the melilite + diopside + liquid volume in the facet V–H–G–W and against the spinel + diopside + liquid volume in the facet V–H–I–X. These facets only extend part way back to the section nepheline–larnite–forsterite–silica, before being replaced by the facet diopside + plagioclase + nepheline + liquid, N–G–H–I–M. The diopside + melilite + liquid volume that abuts against the diopside + plagioclase + liquid volume in the lower left front of the figure is separated from it at the lower left/back by a wedge-shaped diopside + nepheline + liquid volume PNMKJIHG.

A triangular prism shaped volume of diopside + spinel + liquid V–X–Y–J–H–I terminates against the diopside + nepheline + liquid volume in the facet J–H–I. The diopside + nepheline + liquid and diopside + forsterite + liquid volumes abut in the facet I–J–K–M.

G, H, I, and J are the inferred univariant equilibria of the five-component system. The choice is not unique and represents a judgement based upon the improbability of diopside + plagioclase + melilite + forsterite becoming stable with falling temperature prior to the diopside + nepheline + liquid volume being encountered.

The section nepheline–anorthite–diopside (Schairer, Tilley, and Brown, 1967) intersects as piercing points (pseudo-quaternary isobaric invariant points) $^5E^2_{di,\ plag,\ ne,}$

$_{fo,\ 1}$ (IM of fig. 14 and F' of Schairer, Tilley, and Brown, 1967, fig. 70), $^5E^2_{di,\ ne,\ fo,\ mel,\ 1}$ (JK of fig. 16 and C' of Schairer, Tilley, and Brown, 1967, fig. 70), and $^5E^2_{di,\ ne,\ mel,\ plag,\ 1}$ (GH of fig. 14 and L of Schairer, Tilley, and Brown, 1967, fig. 70) and also intersects a thermal divide on $^5E^3_{ne,\ di,\ fo,\ 1}$ (I J K F M of fig. 14). A, B (dotted lines) are thermal divides on $^5E^3_{di,\ plag,\ wol,\ 1}$ and $^5E^3_{di,\ plag,\ fo,\ 1}$, respectively, separating an upper region of the figure where fractional crystallization leads to silica-rich end points from a lower region where fractional crystallization leads to silica-poor end points. Schairer and Yoder (personal commun.) have encountered the equilibria GW, GP, and GN of figure 14 in studies on the section albite-anorthite-akermanite.

C is a thermal divide on $^5E^3_{di,\ plag,\ tr,\ 1}$ which with B separates a righthand portion of the diagram in which fractional crystallization leads to orthopyroxene-bearing end points from a left hand portion in which fractional crystallization leads to wollastonite, nepheline, or melilite bearing end points.

D is a thermal divide on $^5E^3_{di,\ mel,\ plag,\ 1}$ which in the system CMAS prevents the continued fractionation and continued calcium enrichment of liquids that have entered the diopside + spinel + melilite-bearing equilibria after possible derivation from parental liquids near divide B on $^5E^3_{di,\ plag,\ fo,\ 1}$. This divide does not extend as far into the system as the section nepheline–larnite–forsterite–silica, but then there is a divide, F, on $^5E^3_{di,\ ne,\ fo,\ 1}$ preventing access to melilite-bearing end points from liquids commencing near the divide B on $^5E^3_{di,\ plag,\ fo,\ 1}$ or indeed from any diopside + plagioclase-precipitating liquid.

The nature and temperature relationships of the univariant equilibria of the five-component system $^5E^1_{di,\ plag,\ wol,\ mel,\ ne,\ 1}$ (G), $^5E^1_{di,\ plag,\ mel,\ ne,\ sp,\ 1}$ (H), $^5E^1_{di,\ plag,\ fo,\ ne,\ sp,\ 1}$ (I), and $^5E^1_{di,\ mel,\ sp,\ fo,\ ne,\ 1}$ (J) are unknown, nor is it known whether the divariant equilibria $^5E^2_{di,\ plag,\ ne,\ mel,\ 1}$ (G-H), $^5E^2_{di,\ plag,\ ne,\ sp,\ 1}$ (H-I), $^5E^2_{di,\ mel,\ ne,\ sp,\ 1}$ (H-J), and $^5E^2_{di,\ sp,\ ne,\ fo,\ 1}$ (I-J) possess thermal divides, but it is possible that these equilibria may permit the derivation of liquids to the silica-poor melilite-bearing side of divide F from parental liquids near the divide B.

One way in which this might be possible is if liquids approach $^5E^1_{di,\ plag,\ ne,\ fo,\ sp,\ 1}$ (I) by way of $^5E^3_{di,\ plag,\ fo,\ 1}$ *en route* from the thermal divide B; there lose plagioclase and continue fractionation in $^5E^2_{di,\ ne,\ fo,\ sp,\ 1}$ (I-J), lose spinel by reaction in $^5E^1_{di,\ ne,\ fo,\ sp,\ mel,\ 1}$ (J), and then proceed by $^5E^2_{di,\ ne,\ fo,\ mel,\ 1}$ (J-K). $^5E^2_{di,\ ne,\ fo,\ mel,\ 1}$ certainly involves reaction between olivine and liquid at piercing point K, hence somewhere between J and K strongly fractionated liquids will leave this equilibrium via $^5E^3_{di,\ ne,\ mel,\ 1}$ (surface K–J–H–G–P) *en route* to wollastonite-bearing end points, from which a return to plagioclase-bearing conditions may be possible.

If such behavior is possible and it extends into the more complex natural basalt system, then it may prove to be an essential feature in the derivation of the melilite nephelinites from parental alkali olivine basalt magmas by low pressure fractionation. Failing some such mechanism these melilite-bearing rocks must be regarded as owing their origin partly to an essential high-pressure event, whatever the extent of their subsequent compliance with low-pressure equilibria.

Finally attention is drawn to the pronounced depression of the temperatures of equilibria and thermal divides by addition of Na_2O to the system, as illustrated by the temperatures indicated in figure 14.

SUMMARY AND CONCLUSIONS

Diopside and spinel are in equilibrium at the solidus in the system CaO-MgO-Al_2O_3-SiO_2 and the easily produced alternative assemblage anorthite + forsterite + melilite is metastable. Revisions of previously published results are noted.

Three univariant (isobaric invariant) equilibria involving diopside, spinel, liquid, and any two of anorthite, forsterite, and melilite exist at atmospheric pressure. In one, anorthite and forsterite are in reaction relationship with silica undersaturated liquid while in another forsterite alone is in reaction relationship with the liquid.

The existence of anorthite-liquid and forsterite-liquid reaction relationships potentially gives rise to the development of diopside, spinel, and melilite precipitating liquids from parental liquids precipitating

anorthite, diopside, and forsterite, which may be relevant to the genesis of melilites and melilite-nephelinites from parental alkali olivine basalt magma at low pressure. The system CaO–MgO–Al_2O_3–SiO_2 does not present a close analogy to natural silica-undersaturated basic magmas however because of the presence of spinel in the important equilibria and of a thermal divide preventing further evolution toward wollastonite-bearing end points. The section nepheline–larnite–forsterite–silica of the system Na_2O–CaO–MgO–Al_2O_3–SiO (Schairer and Yoder, 1964) does not contain diopside + spinel equilibria, does not contain a thermal divide preventing access to wollastonite-bearing end points, and does contain the olivine-liquid reaction relationship in silica-poor liquids which is one of the essentials for deriving melilite-nephelinites from alkali-olivine basalts by low-pressure fractional crystallization. However, it does not contain any plagioclase-liquid reaction relationships resulting in the loss of plagioclase as a phase during fractional crystallization which are equally essential for this derivation, and it does contain a thermal divide preventing access to melilite-bearing equilibria from diopside + plagioclase + olivine-bearing equilibria.

Consideration of relationships in the system Na_2O–CaO–MgO–Al_2O_3–SiO_2 between the sections CaO–MgO–Al_2O_3–SiO_2 and nepheline–larnite–forsterite–silica suggests that all the equilibria required to evade the divides and lose both olivine and plagioclase to permit the derivation of melilite-nephelinites by the low-pressure extreme fractional crystallization of alkali-olivine basalt magma may well exist in what is essentially the per-aluminous portion of the five-component system, without recourse to per-alkaline conditions or high-pressure events.

This study was supported by the Natural Environment Research Council.

Appendix

Preparation of gel compositions.—Gelled compositions in systems containing CaO, MgO, Al_2O_3, and SiO_2 were prepared by mixing the required weights of standard solutions of calcium, magnesium, and aluminium nitrates. Sufficient ethanol was added to ensure complete miscibility with the required amount of tetraethyl orthosilicate (TEOS) as a source of silica, and the mixture gelled by the addition of concentrated ammonia.

Ammonia precipitates first the aluminium hydroxide followed by magnesium hydroxide as a gelatinous product in which the calcium and silica (TEOS) are distributed. Slow additions of ammonia were not satisfactory as clots of aluminium hydroxide which were not broken up by mechanical agitation formed, but a rapid addition of excess ammonia produced a gel that thickened rapidly and prevented differentiation. The TEOS was hydrolyzed slowly by the excess ammonia. After drying the gel was roasted and ground to give a fine grained crystalline product.

Experimental.—The nitrate solutions of aluminum and magnesium were prepared at concentrations safely below the solubility of the nitrates at room temperature. Calcium nitrate was prepared at a similar concentration for convenience. Details of the starting materials and solution strengths appear on page 389. In each case the starting material and some deionized water were cooled in an ice bath, and a capillary drip feed of 45 percent AnalaR nitric acid added. After violent reactions had ceased some solutions, notably aluminum, required digestion at 70 to 90°C for 48 hours to achieve complete solution. The solutions were made up in volumetric flasks although it was found more convenient to weigh at the same time and make up the mixtures on a weight basis. Burettes were used, and the reading noted as a safety check on the weighings.

Materials used

	Material	Final solution strengths (approx) % HNO_3	% oxide
$CaCO_3$	AnalaR, powder dried at 450°C	2	8
Mg	Spectrographical pure crystals	5	8
Al	99.99% dust	20	4
TEOS	recovering of silica determined for each batch and a correction factor applied.		

A 10 gm batch of each composition was made by weighing the required amounts of the various solutions into a 500 ml polythene container with an air-tight lid, the volumes added being noted. Forty ml ethanol were added followed by a weighed quantity of TEOS. After thorough mixing an excess of 0.88 NH_4OH was added, and a thick gel was immediately formed. The air-tight lid was quickly fitted, and the gel left at least overnight to achieve complete hydrolysis of the TEOS.

The gel was then transferred to a 250 ml glass beaker using mixed ethanol water wash liquid and dried out over 2 to 4 days at 75°C. The dry gels were slowly heated to 200°C driving off much of the ammonium nitrate and then heated for 2 hours at 300°C and a further 2 hours at 500°C. After transfer of the gel to a Palau basin removal of volatiles and nitrates was completed in 2 hr at 900°C, and the yield was weighed. The sample was ground for 10 min in an amalgamator, transferred to a platinum crucible, and heated in air at temperatures up to 1150°C for up to 48 hours to produce a principally crystalline product. The crystalline assemblage frequently contained metastable pyroxene, melilite, and monticellite phases.

A recovery of 9.97 to 10.01 g was regarded as acceptable, and the metal nitrate solutions each yielded 9.97 to 10.01 g of the oxide when treated in the manner described. The yield of SiO_2 from TEOS was determined for each batch, values of 99.5 to 99.7 percent of the theoretical value being recorded. A correction factor was used in calculating the required addition of TEOS.

Each sample made up was thought to contain within ± 0.1 percent of the desired amount of each component. One sample was analyzed by Dr. E. L. P. Mercy with the following result:

	Desired	Determined	Apparent Difference
CaO	19.36%	19.22%	—0.14%
MgO	12.76%	12.80%	+0.04%
Al_2O_3	5.87%	6.08%	+0.21%
SiO_2	62.01%	61.81%	—0.20%
Na_2O	nil	<80 ppm	
Fe	nil	<130 ppm	

In view of the uncertainties of silicate analysis this measure of agreement was taken as satisfactory. Na_2O was determined in six other samples by M. J. Saunders, and the range of values was 150 to 290 ppm.

References

Boyd, F. R., and Schairer, J. F., 1964, The system $MgSiO_3$–$CaMgSi_2O_6$: Jour. Petrology, v. 5, p. 275-309.

Chinner, G. A., and Schairer, J. F., 1962. The join $Ca_3Al_2Si_3O_{12}$–$Mg_3Al_2Si_3O_{12}$ and its bearing on the system CaO–MgO–Al_2O_3–SiO_2 at atmospheric pressure: Am. Jour. Sci., v. 260, p. 611-634.

De Neufville, J., and Schairer, J. F., 1962, The join diopside—Ca Tschermak's molecule at atmospheric pressure: Carnegie Inst. Washington Year Book 61, p. 56-59.

De Wys, E. C., and Foster, W. R., 1958, The system diopside–anorthite–akermanite: Mineralog. Mag., v. 31, p. 736-743.

Keith, M. L., and Schairer, J. F., 1952, The stability field of sapphirine in the system MgO–Al_2O_3–SiO_2: Jour. Geology, v. 60, p. 181-186.

Kushiro, I., and Yoder, H. S., 1966, Anorthite-forsterite and anorthite-enstatite reactions and their bearing on the basalt-eclogite transformation: Jour. Petrology, v. 7, p. 337-362.

MacGregor, I. D., 1965, Stability fields of spinel and garnet–peridotites in the synthetic system $MgO–CaO–Al_2O_3–SiO_2$: Carnegie Inst. Washington Year Book 64, p. 126-134.

Muan, A., and Osborn, E. F., 1965, Phase equilibria among oxides in steel making: London, Pergamon Press, 236 p.

O'Hara, M. J., and Schairer, J. F., 1963, The join diopside-pyrope at atmospheric pressure: Carnegie Inst. Washington Year Book 62, p. 107-115.

Osborn, E. F., De Vries, R. C., Gee, K. H., and Kraner, H. M., 1954, Optimum composition of blast furnace slag as deduced from liquidus data for the quaternary system $CaO–MgO–Al_2O_3–SiO_2$: Jour. Metals, Jan. 1954, p. 33-44.

Osborn, E. F., and Tait, D. B., 1952, The system diopside–forsterite–anorthite: Am. Jour. Sci., Bowen v., p. 413-433.

Schairer, J. F., and Kushiro, I., 1965, The join diopside-spinel at atmospheric pressure and the significance of the diopside-spinel assemblage: Carnegie Inst. Washington Year Book 64, p. 100-103.

Schairer, J. F., Tilley, C. E., and Brown, G. M., 1967, The join nepheline-diopside-anorthite and its relation to alkali basalt fractionation: Carnegie Inst. Washington Year Book 66, p. 467-471.

Schairer, J. F., and Yoder, H. S., Jr., 1964, Crystal and liquid trends in simplified alkali basalts: Carnegie Inst. Washington Year Book 63, p. 65-74.

Yoder, H. S., Jr., and Chinner, G. A., 1960, Grossularite–pyrope–water system at 10,000 bars: Carnegie Inst. Washington Year Book 59, p. 78-81.

Yoder, H. S., Jr., and Tilley, C. E., 1962, Origin of basalt magmas: an experimental study of natural and synthetic rock systems: Jour. Petrology, v. 3, p. 342-532.